May 17th, 8:20 AM

3D CFD Modeling of a Supercritical Bottom Rack Intake

S.N. Chan
Hong Kong University of Science and Technology, treechansn@ust.hk

Joseph H.W. Lee
Hong Kong University of Science and Technology, jhwlee@ust.hk

Recommended Citation

Chan, S.N. (2018). 3D CFD Modeling of a Supercritical Bottom Rack Intake. Daniel Bung, Blake Tullis, 7th IAHR International Symposium on Hydraulic Structures, Aachen, Germany, 15-18 May. doi: 10.15142/T31D2J (978-0-692-13277-7).

7th International Symposium on Hydraulic Structures Aachen, Germany, 15-18 May 2018
ISBN: 978-0-692-13277-7 DOI: 10.15142/T31D2J

3D CFD Modeling of a Supercritical Bottom Rack Intake

S.N. Chan[1,2] & J.H.W. Lee[1]
[1]*Department of Civil and Environmental Engineering, Hong Kong University of Science and Technology, Hong Kong, China*
[2]*Institute for Advanced Study, Hong Kong University of Science and Technology, Hong Kong, China*
E-mail: treechansn@ust.hk

Abstract: *Compact intake structures are used for diverting turbulent supercritical flow on steep catchments in the hinterland of the urban area of Hong Kong to an underground flood diversion system through a number of vortex dropshafts. Bottom racks are placed at the entrance of the intake to exclude debris from entering the system. The rack bars interact with the supercritical inflow and creates a highly turbulent air-water mixture. This paper presents a three-dimensional (3D) Computational Fluid Dynamics (CFD) modeling study to predict the complex flow details and air concentration of the bottom rack intake structure, using the Volume-of-Fluid (VOF) technique. Numerical simulations are conducted with different inflow rates and bottom rack bar shapes. The water depth, velocity, and air concentration agree well with experimental measurement. Model results show that the rack interception induces an energy loss and increases the flow depth above the rack. The rack interception also gives rise to a sheet jet beneath the rack and results in air entrainment. In the rack chamber, the flow consists of a wall jet that impinges on a spiral circulation of aerated flow, inducing significant turbulence and air entrainment. The average air concentration in the rack ranges from 20% - 50% and decreases with increasing discharge.*

Keywords: *Intake structure, supercritical flow, bottom rack, volume-of-fluid, CFD*

1. Introduction

To alleviate flooding and increase flood protection standards, a storm water runoff interception and transfer scheme has been designed and constructed in the steep hinterland of the urban area of Hong Kong. This scheme involves the interception and transfer of flood flows to the sea via a 10.54 km drainage tunnel, fed by 34 intake shafts positioned across the catchment basin (DSD 2003; Lee et al. 2005). The intake structures and the dropshafts are designed based on site condition to convey a flood with a 200-year return period (18 m^3/s). The intakes are located on steep watercourses (average slope of 40%) with supercritical flow in a storm. During significant storm events, stream flows often carry sediments, boulders, and/or debris, which would adversely affect the operation of the drainage tunnel system. A screened intake with bottom racks is used to prevent the ingress of debris. The intercepted flow is then passed into the dropshaft via a bottom rack chamber, which changes the flow direction by 90 degrees (due to site constraints), and a vortex inlet. The vortex inlet facilitates energy dissipation and the development of a central air core within the dropshaft. Both upstream of the bottom rack intake or within the structure, the flow cannot be fully stilled because of site constraints; the intercepted flow remains supercritical throughout the structure.

A bottom rack is a hydraulic structure, essentially consisting of an opening in the channel bottom, covered with an arrangement of metal racks to prevent the transport of debris or sediment through the opening. Bottom rack is extensively used for hydropower, water supply, and irrigation, mainly in areas with steep terrain and gravel river beds (e.g., Subramanya 2009). Nevertheless, previous studies are mainly concerned with sub-critical approach flows (e.g., Mostkow 1959; Brunnela et al. 2003; Righetti and Lanzoni 2008; Kumar et al. 2010).

The present bottom rack chamber design was derived from a comprehensive physical model investigation (Lee et al. 2005a) and is significantly different from standard bottom rack intake designs in several ways. Previous studies mainly focus on typical bottom rack intakes with a free overfall. The flow plunges to the collection chamber after rack interception. However, in the present study, the flow in the entire structure is supercritical and remains an open channel flow at rack interception. The water plunges onto the underlying supercritical flow below, and the rack bars create complex flow features, such sheet jets, beneath the bars. In addition, the rack chamber is relatively compact and designed to divert the supercritical inflow with energy dissipation. The flow inside the chamber is highly turbulent, aerated, and three-dimensional. Such complex turbulent aerated flows in the bottom rack chamber have not been systemically studied.

In recent years, attempts have been made to tackle the air-water flow in hydraulic structure problems using Computational Fluid Dynamics (CFD) models, in particular on stepped spillways (Bombardelli et al. 2011; Bayon et al. 2017). With the Volume-of-Fluid (VOF) method, the interface between the water and air can be located and tracked when it moves through the computational domain. For bottom rack intakes, Wong (2009) attempted a CFD simulation on a supercritical bottom rack chamber using FLOW3D; however, due to coarse grid resolution, the details at the rack interception cannot be resolved. Castillo et al. (2013) use VOF method to simulate the flow from a subcritical bottom rack and validated it with experimental data. There lacks systematic experimental and numerical studies for supercritical bottom rack flow and the air-water interaction in a compact bottom rack chamber for a vortex intake structure. This paper presents a first time systematic numerical study on the hydraulics of a supercritical bottom rack intake using a three-dimensional (3D) CFD model. First, the numerical model set-up will be presented. Then the computational model results will be validated against experimental data, and the air-water flow in the bottom rack intake will be discussed.

2. Numerical Model

The CFD model of the bottom rack intake is developed according to a 1:9.5 Froude scale physical model of the prototype design of the Hong Kong West Drainage Tunnel diversion scheme (Lee et al. 2005; Wong 2009). The model comprises an approach channel of length 920 mm and uniform width 316mm, the bottom rack of length 1084mm and the underlying chamber, the link channel, and the spiral vortex intake with dropshaft (Fig. 1). The inflow is fed from an inflow head tank and the flow rate is measured using an ultrasonic flowmeter. The flow leaves the inflow tank and runs down the 1:2.5 slope approach channel to the downstream structures. This supercritical flow is intercepted by a bottom rack in 1:5 slope. The channel flow beneath the rack runs to a curved-bottom channel at the entrance to the bottom rack chamber. After the bottom rack chamber, the flow is diverted to a spiral vortex intake structure via the link-channel and collected by an underground sump and recirculated. Flow depth and velocity were measured using a point gauge and a propeller current meter respectively. Air concentration in the channel and chamber flow is measured using both dual-tip optical probes and single-tip conductivity probes. Rack bars of various cross-sectional shapes are tested in the experiments. Measurement is made in particular for circular racks made of 12.1mm diameter bars with 22.6mm center-to-center separation and diamond racks made of 8.4 × 8.4mm square bars with 23mm center-to-center separation. Details of the experimental design and measurement techniques can be found in Wong (2009).

The CFD model is developed based on the commercial code of ANSYS FLUENT (ANSYS 2013), using the VOF method to model two immiscible fluids (water and air) by solving a single set of momentum equations and tracking the volume fraction of each of the fluids throughout the domain (Hirt and Nichols 1981). The tracking of the interface between the phases is accomplished by the solution of a continuity equation for the volume fraction of water α_w:

$$\frac{\partial}{\partial t}(\alpha_w \rho_w) + \nabla \cdot (\alpha_w \rho_w \boldsymbol{U}) = 0 \tag{1}$$

where $\boldsymbol{U}$ is the phase-averaged air-water mixture velocity. A single momentum equation is solved throughout the domain, and the resulting velocity field is shared among the phases:

$$\frac{\partial}{\partial t}(\rho \boldsymbol{U}) + \nabla \cdot (\rho \boldsymbol{U}\boldsymbol{U}) = -\nabla P + \nabla \cdot [\mu_t (\nabla \boldsymbol{U} + \nabla \boldsymbol{U}^T)] + \rho \boldsymbol{g} \tag{2}$$

where P is the pressure and $\boldsymbol{g}$ = (0, 0, -9.81) m/s^2 is the gravitational acceleration; the phase-averaged density $\rho = (1 - \alpha_w)\rho_a + \alpha_w \rho_w$ is determined from the air (ρ_a = 1.225 kg/m^3) and water densities (ρ_w = 998.2 kg/m^3) through their volume fraction; the turbulent dynamic viscosity μ_t is determined using the Re-Normalisation Group (RNG) k-ε turbulence model (Yakhot et al. 1992). Since the dynamics of both air and water are solved, a semi-empirical model of air entrainment from the water surface, like that used in FLOW-3D (Hirt, 2003), is not required. The governing equations are solved numerically using the finite volume method embedded in the FLUENT code (ANSYS 2013). Solution convergence is declared when the normalized residual is less than 10^{-4} for continuity, velocity, volume fraction of water, and the turbulence quantities of k and ε. About 10 iterations are required for convergence in each time step.

The CFD modeling focuses on the experiments with circular and diamond shaped rack bars, as they are considered more optimal designs compared to bars with other shapes (Wong 2009). An unstructured boundary-fitted model grid is used for the numerical simulation (Fig. 1). The computational mesh sizes vary from 67,840 for cases without rack to 347,520 for cases with circular rack bars. Mesh refinement is made to near the bed and the region of bottom rack (Fig. 1). The minimum grid size is 1 mm. The vortex intake and its linkage channel are not modeled.

The computational model has four open boundaries—the inflow, the outflow to link channel for the vortex dropshaft, the overflow outlet to the original channel, and the top atmospheric boundary (Fig. 1). The upstream inlet of the approach channel is prescribed with the total water flow rate and the critical depth of the flow. The top atmospheric boundary of the CFD model is prescribed with zero pressure. The outlets of overflow channel and the link channel are prescribed with zero gauge pressure as the water depths at the two locations are not known beforehand. A roughness height of 0.01mm is prescribed for all wall boundaries.

The model run starts with an initially dry condition. The supercritical flow in the approach channel and the bottom rack chamber develops from the inlet with a time step of 0.0005 to 0.001 s. The initial start-up period is about 10s; afterwards, the model prediction can be considered as quasi-steady. About 20s of quasi-steady state solution, at a time interval of 0.1s, is used for evaluating the time-averaged properties of flow depth, velocity, and air concentration. Numerical simulations are performed for the representative flow rates 21.6 L/s, 41.3 L/s, and 70.5 L/s. The run time for 20s of flow is about 120 hours for cases with bottom rack on a workstation with an Intel 3.4 GHz CPU with quad-core parallel computation.

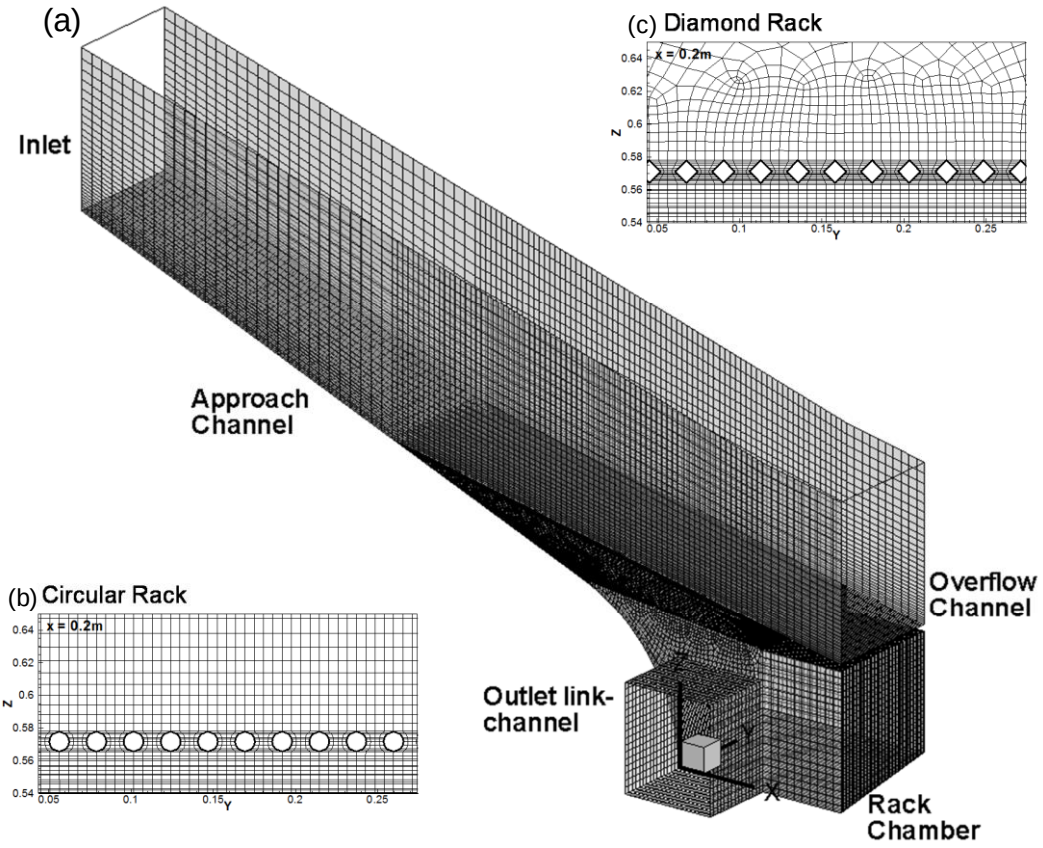

Figure 1. (a) Computational mesh of the laboratory model on supercritical bottom rack intake. (b), (c) mesh details at the cross section of rack bars.

3. Results and Discussions

3.1. Flow profile

Fig. 2a shows the observed bottom rack flow in the experiments. The flow profile upstream of the bottom rack follows that of a typical S2 curve (from critical depth to normal depth). The flow can run through the rack smoothly without choking or jump above the rack. Downstream of the leading edge of the bottom rack (s = 0, s is the coordinate along the slope of main channel), the flow is intercepted; the flow enters the rack chamber in the space between the rack bars. The flow above the rack is a spatially varied flow as the discharge (above the rack) decreases with s. The rack

interception length L_w is defined as the distance between the upstream leading edge of the rack and the point where the free surface flow intersects the rack (Fig. 2a).

Fig. 2b compares the predicted flow depth along the channel in the presence of bottom rack bars and in the case without them. Without the rack, the water surface is parallel to the channel bed. In the presence of rack bars, the flow depth rises higher than the one without rack and appears to be asymptotic to the slope of the bar until it intercepts with the bar. In general, before rack interception, the flow depth of "between the rack" and "above the rack" are the same. There is a slight difference between the flow "between the rack" and the flow diverted "above the rack" at the end of L_w. At the middle of L_w, the flow depth is increased by around 8% - 22%, due to the energy loss induced by the flow contraction when it passes through the rack. Near the end of L_w, the flow depth between the rack drops rapidly because the flow leaves between the bars. CFD prediction of the free surface level (defined as 50% air concentration) shows a good comparison with the measured water level. Both measurement and CFD prediction show that circular rack bars produce the smallest L_w for all three flow rates, while the L_w of diamond bars is slightly larger (not shown).

When the flow has passed through the rack, the flow consists of two streams: (a) attached-rack flow and (b) main channel flow. After the main flow leaves the rack, a certain amount of the flow is running along the surface of the bottom rack before leaving the rack—the attached rack flow. The flow leaves the rack at high speed and forms the sheet-jet beneath the rack. Disintegration of this thin sheet jet in air can be observed as it plunges onto the main channel flow (Fig. 2a). The flow surface is very irregular as the water sheet-jet plunges from the top surface. The CFD predicted mean water level between the rack bars are lower than that directly beneath the bars, as the flow velocity between the bars are higher (Fig. 2b).

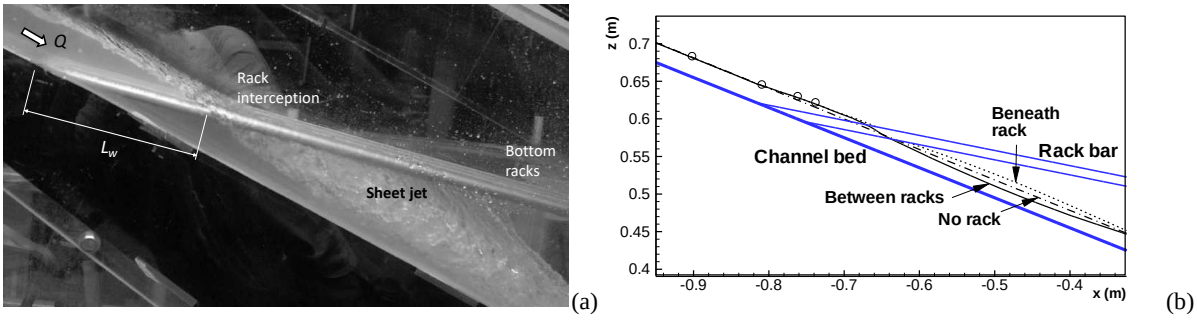

Figure 2. (a) Observed flow profile, circular rack bars, (b) CFD predicted flow (Q = 45.4 L/s, circular rack). Predicted free surface is represented by the 50% air concentration line. Circular symbols are measured free surface before the rack.

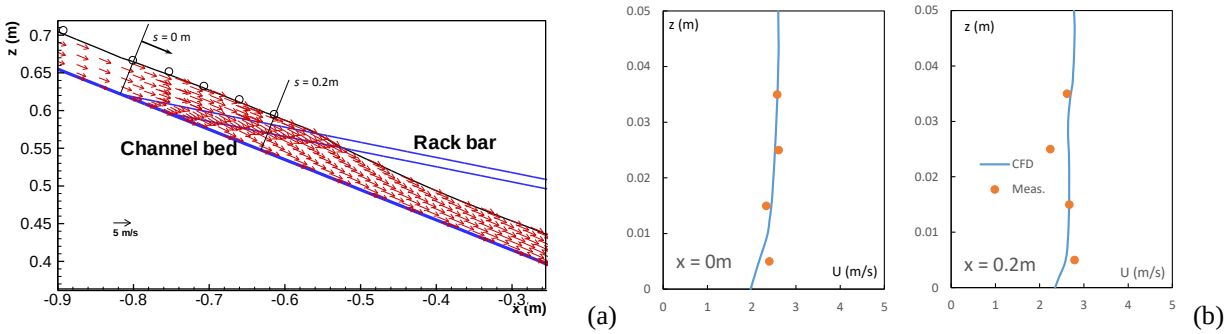

Figure 3. (a) CFD predicted velocity field along the channel centerline and between racks (Q = 41.3 L/s, circular rack). (b) Comparison of predicted and measured velocity at cross sections of s = 0m and s = 0.2m from the rack interception.

3.2. Flow Field

The entire bottom rack flow can be illustrated by the predicted velocity in Fig. 3a for a medium flow condition (Q = 41.3 L/s) between the rack bars. The supercritical open channel flow is intercepted by the rack, with a slight increase in depth due to the contraction in flow area at rack interception. The flow contraction and expansion at the rack opening induces energy dissipation. The maximum velocity occurs when the flow leaves the rack. After the rack interception, the clear water flow runs along the main channel with a decreased flow depth with a zone of air-water

mixture; due to the sheet flow plunging from the rack bars, flow velocity increases. The depth profile is essentially similar for different rack types. The CFD prediction compares well with the measured flow velocity (Fig. 3b).

3.3. Air-Water Flow After Rack Interception

Fig. 4a shows the predicted air concentration (air volume fraction) profile at the rack interception for Q = 41.3 L/s with the circular rack. The bottom layer of the main channel flow is in clear water (c = 0). Above the clear water layer (around 30mm), the air concentration increases to 1 over a transition layer (15-20mm) of air-water mixture that grows with distance from rack interception. The falling sheet jet generates splashing and air entrainment after rack interception. The air concentration in the complex and highly fluctuating flow is resulted from the entrained air, the unsteady nature of the jet-water boundary of the sheet jet and underflow, and droplets from splashing and flow impingement.

Fig. 4b shows the flow feature and average air concentration distribution in the bottom rack chamber for Q = 41.3 L/s. The average air concentration distribution at the bottom rack chamber can be evaluated by averaging the predicted air volume fraction at a snap-shot interval of 0.1s for a total simulation period of 10s as a quasi-steady flow. Upstream of the bottom rack, the free surface is predicted as uniform with little air entrainment. The flow intercepts the rack smoothly and runs down the curved channel. Due to acceleration, change of flow direction and air entrainment, the flow inside the bottom rack chamber is three-dimensional, highly turbulent, and aerated. An anti-clockwise flow field is formed in the bottom rack chamber. The air concentration in the bottom rack chamber is highly non-uniform and unsteady, but, on average, it is higher at the interception point between the curved channel and the chamber due to air entrainment. The flow pattern and air concentration appear to be little affected by the presence and the cross-sectional shape of rack bars (not shown).

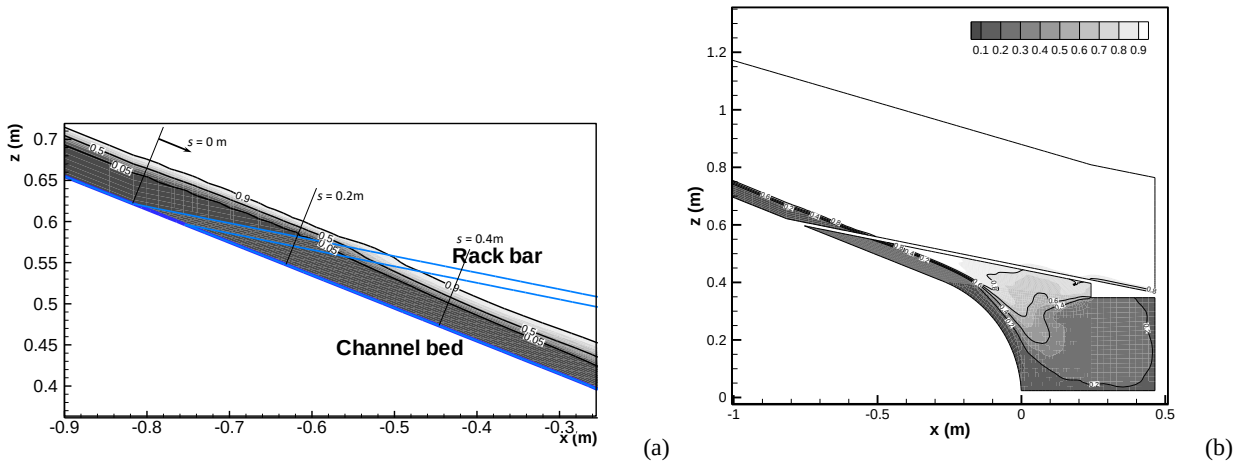

Figure 4. (a) CFD predicted air concentration (air volume fraction) between rack bars, (b) predicted average air concentration at the centerline of bottom rack chamber (Q = 41.3 L/s, circular rack).

4. Conclusions

A 3D CFD model with VOF technique has been developed to study the hydraulics of a supercritical bottom rack intake. The model results are validated with detailed laboratory experimental measurement. Model simulation shows that the supercritical flow depth above the rack increases with downstream distance due to energy loss, resulting from the flow contraction and expansion during flow passage through the racks. When the flow nearly passes the rack, the flow depth decreases abruptly, and the three-dimensional effect plays an increasingly dominant role. After the rack interception, the flow is characterized as a sheet jet flow beneath the racks plunging onto the main channel flow. The flow in the rack chamber consists of a wall jet impinging onto a spiral circulation flow in the chamber. The jet impingement gives rise to significant turbulent kinetic energy and air entrainment.

CFD prediction of major flow feature and air concentration compares well with experimental measurement, despite the detailed flow feature around the rack bars, such as the sheet jet, cannot be satisfactorily resolved by the current

grid resolution. The complex spatial air concentration distribution for different discharges are satisfactory predicted, showing the applicability of a 3D CFD model for this complex air-water phenomenon.

5. Acknowledgements

This study was supported by the Drainage Services Department of the Hong Kong SAR Government and in part by a grant from the Hong Kong Research Grants Council (RGC 714306).

6. References

ANSYS Inc. (2013). ANSYS FLUENT 15.0 Theory Guide.

Bayon, A., Toro, J.P., Bombardelli, F.A., Matos, J., and Lopez-Jimenez, P.A. (2017). "Influence of VOF technique, turbulence model and discretization scheme on the numerical simulation of the non-aerated, skimming flow in stepped spillways." *Journal of Hydro-environment Research*.

Bombardelli, F.A., Meireles, I., and Matos, J. (2011). "Laboratory measurements and multi-block numerical simulations of the mean flow and turbulence in the non-aerated skimming flow region of steep stepped spillways." *Environmental Fluid Mechanics*, 11(3), 263–288.

Brunella, S., Hager, W.H., and Minor, H.E. (2003). "Hydraulics of bottom rack intake." *Journal of Hydraulic Engineering*, ASCE, 129(1), 2-10.

Castillo, L.G., Carrillo, J.M., and García, J.T. (2013). "Flow and Sediment Transport through Bottom Racks. CFD Application and Verification with Experimental Measurements." Proceedings of *2013 IAHR Congress*, Chengdu, China, Sep 2013. Tsinghua University Press, Beijing, China.

Drainage Service Department (DSD) (2003). Stormwater Drainage Master Plan Study in Northern Hong Kong Island – Executive Summary. The Government of Hong Kong Special Administrative Region, China.

Hirt C.W. (2003). Modeling Turbulent Entrainment of Air at a Free Surface. FSI-03-TN61-R. Flow Science, Inc.

Hirt, C.W., and Nichols, B.D. (1981). "Volume of fluid (VOF) method for the dynamics of free boundaries." *Journal of Computational Physics*, 39(1), 201-225.

Kumar, S., Ahmad, Z., Kothyari, U.C., and Mittal, M.K. (2010). "Discharge characteristics of a trench weir." *Flow Measurement and Instrumentation*, 21, 80-87.

Lee, J.H.W., Yu, D., Chan, H.C., Gore, L., and Ackers, J. (2005). "Bottom rack intake for supercritical storm flow diversion on steep urban catchment." *The 31st IAHR World Congress*, Seoul, Korea, 11-16 September 2005. The International Association for Hydro-Environment Engineering and Research.

Mostkow, M.A. (1959). "Theoretical study of bottom type water intake." *La Houille Blanche*, 4, 570-580.

Righetti, M., and Lanzoni, S. (2008). "Experimental study of the flow field over bottom intake racks." *Journal of Hydraulic Engineering*, ASCE, 134(1), 15-22.

Subramanya, K. (2009). Flow in Open Channels. Tata McGraw-Hill, New Delhi, 3rd edition.

Wong, K.C. (2009) Hydraulics of Bottom Rack Chamber for Supercritical Flow Diversion. M.Phil Thesis. The University of Hong Kong, Hong Kong, China.

Yakhot, V., Orszag, S.A., Thangam, S., Gatski, T.B., and Speziale, C.G. (1992). "Development of turbulence models for shear flows by a double expansion technique." *Physics of Fluids A*, 4(7), 1510-1520.